On the Representation of Through-the-Thickness Reinforcements in Finite Element Analysis of Stitched, Blade Stiffened Panels

ABSTRACT

Modern aircraft employ laminated composites for their tailorable in-plane properties, high specific strengths, and high specific stiffnesses. However, laminated composites exhibit relatively poor interlaminar properties without through-the-thickness reinforcements. Quantifying the necessary amount of through-the-thickness reinforcements is necessary to reduce cost and meet damage tolerance certification requirements. In this study, a discrete superposed cohesive element (DSCE) approach is applied to represent the mixed-mode delamination behavior of stitched stiffened panels subjected to seven-point bending. This approach is compared to a one-dimensional embedded spring element (ESE) method. The DSCE approach uses two superposed bilinear traction-separation laws to obtain a representative load-displacement response determined from interlaminar tensile and shear tests. Additionally, several stitch configurations (unstitched, stitched, and overstitched) are evaluated in terms of their load-displacement response and crack-arrestment capability. Results indicate that the DSCE and ESE approaches show good agreement with respect to the predicted load-displacement response, but the ESE method tends to overpredict the crack growth behavior by approximately 13%. Stitches were not observed to fail during skin-stringer separation. Using an overstitched laminate with stitches near the flange edge provides the greatest crack-arrestment capability. Furthermore, the skin retains 92% of its stiffness after skin-stringer separation occurs.

INTRODUCTION

Highly unitized, integral, and lightweight composite structures are essential in the aerospace industry to improve payload capacity, aircraft range, and fuel efficiency. Traditionally, laminated composites are fabricated with in-plane fiber-reinforced plies that are infused and subsequently cured with a polymer matrix. Each layer of reinforcements is tailored in a planar direction to achieve the required axial, bending,

---

Daniel A. Drake, Analytical Mechanics Associates, Inc., Hampton, VA 23681, U.S.A.
Kyongchan Song, NASA Langley Research Center, Hampton, VA 23681, U.S.A.
W. Allen Waters, Analytical Mechanics Associates, Inc., Hampton, VA 23681, U.S.A.
Andrew E. Lovejoy, NASA Langley Research Center, Hampton, VA 23681, U.S.A.

and twisting stiffnesses needed for part operation. However, laminated composites exhibit relatively low interlaminar properties due to the absence of out-of-plane, or through-the-thickness, reinforcements. Laminated composites without through-the-thickness reinforcements rely on the surrounding polymer matrix to carry out-of-plane stresses, which may lead to damage states such as matrix cracking and delamination.

Through-the-thickness stitching is an increasingly popular method to impede delamination within composite laminates subjected to out-of-plane stresses [1,2]. The stitching process involves sewing thread into a dry fabric preform using a robotic sewing machine prior to resin infusion. Notably, the stitching process may slightly decrease the in-plane mechanical performance by disturbing the in-plane fiber orientations of the composite laminate [1]. However, this reduction in mechanical properties is dependent upon material type (unidirectional, woven, or sandwich) and stitch processing parameters (number of stitches per unit area, or stitch density, and linear thread density) [2]. In recent years, The Boeing Company, United States Air Force, and National Aeronautics and Space Administration (NASA) have developed the Protruded Rod Stitched Efficient Unitized Structural (PRSEUS) design. The PRSEUS design uses a selective stitching approach to join primary structural elements, such as skin, stringers, and frames [3,4]. The reduction of in-plane properties is minimized by stitching only at structural element interfaces where delamination due to mixed mode stresses is critical. It has been shown that through-the-thickness stitches can arrest interlaminar damage that develops from within a PRSEUS panel subjected to tensile loads [3]. From a damage-tolerant design perspective, quantifying the necessary amount and size of stitches required to arrest these damage mechanisms is needed to reduce cost and meet certification requirements.

A common approach to represent a stitch in finite element analysis is to use a spring element. In this case, delamination of a stitched interface is modeled by superposing spring elements with an interlaminar fracture modeling approach, e.g., cohesive elements or a virtual crack closure technique (VCCT) interaction. Typically, a truss or a connector element with released rotational degrees of freedom at each node is used to represent each stitch [5–7]. Individual spring elements can be introduced by sharing nodes with the continuum elements that represent the stitched substrates [6,8,9]. Modification of the mesh density may be necessary to attach each spring element node at the appropriate location. This approach can be time-consuming for the end-user; therefore, the embedded element technique has been proposed as an alternative approach [5,7,10]. The embedded element technique eliminates the requirement for nodal connectivity between the springs and continuum mesh. The spring elements are defined independently of the continuum (host) mesh. If a spring element node is within a host element, its translational degrees of freedom are constrained to the interpolated value of the corresponding degrees of freedom of the host element [5,10].

Spring elements have been widely shown to accurately predict the failure processes of stitches within composite laminates that are subjected to Mode I conditions [7–9]. Stitch failure is typically dictated by the load-displacement response obtained from interlaminar tensile tests containing a single stitch [8,11,12] or multiple stitches [6,7,13]. These stitch failure processes are stitch-matrix debonding, slack absorption, stitch failure, and frictional pullout [8]. Stitches that are subjected to Mode II shear conditions are observed to exhibit unique damage mechanisms [14], such as stitch plowing and flexural splitting, that are not observed in Mode I conditions at the

delaminated interface. These damage mechanisms may not be accurately represented by constitutive relationships determined by interlaminar tensile tests for one-dimensional spring elements. Therefore, alternative approaches may be necessary to predict the physical stitch behavior under shear or mixed-mode stresses.

An alternative approach is to use a discrete cohesive element method to represent through-the-thickness reinforcements [15–18]. Traditional cohesive zone modeling smears the failure process across an entire interface to estimate the corresponding traction stresses and fracture process zone during delamination. The discrete cohesive element approach uses single cohesive elements to represent the failure process of individual stitches during global interface failure between plies. The term "discrete" refers to representing the failure process of the through-the-thickness reinforcement separately from the failure process of delaminating plies. The tensile and shear behavior of the through-the-thickness reinforcement can be related using a power-law or Benzeggagh-Kenane (B-K) fracture criterion. Several authors [15,16] have used a discrete cohesive zone approach with different traction-separation laws for unstitched and stitched cohesive elements at the delaminated interface. A good correlation between the predicted and experimental measurements was observed during Mode I fracture.

Through-the-thickness reinforcements have been widely shown to impede delamination growth within coupon tests such as the double cantilevered beam test [8] or the end-notch flexure test [19]. For certification, progressive failure analyses are often assessed using a building block approach from a coupon level to a structural scale level [20,21]. At the sub-element structural level, the seven-point bend test appears to be an excellent candidate to investigate the influence of stitches to resist interlaminar damage under mix-mode conditions. The seven-point bend test simulates the skin-stringer separation during a post-buckled event of a stiffened panel subjected to in-plane compression [22–24]. In this study, unstitched and stitched composite blade stiffened panels subjected to seven-point bend loads were investigated. A discrete superposed cohesive element (DSCE) method was applied to represent the mixed-mode behavior of through-the-thickness reinforcements that bridge across delaminations. This methodology was compared to a traditional embedded spring element (ESE) method, and their corresponding load-displacement and crack growth responses were evaluated. Two finite element models were developed, one to represent each stitch modeling approach. Additionally, three different stitching configurations, defined as stitched, overstitched, and twice overstitched, were investigated and compared between each modeling approach. This paper presents the computational modeling results that are being used to design the seven-point bend test plan for future testing activities. The modeling approaches, assumptions, and skin-stringer separation characteristics for each unstitched and stitched configuration are discussed in more detail in the following sections.

DESCRIPTION OF FINITE ELEMENT MODELS

Finite element analysis of unstitched and stitched blade-stiffened panels subjected to seven-point loads was performed using Abaqus/Explicit 2021[*] commercial

[*] Specific vendor and manufacturer names are explicitly mentioned only to accurately describe the test hardware. The use of vendor and manufacturer names does not imply an endorsement by the U.S. Government nor does it imply that the specified equipment is the best available.

software [5]. Two separate models were developed, one using the ESE and one using the DSCE method, and are shown in Figures 1(a) and 1(b). The three-dimensional ESE model was developed based on previous research [25]. The width and length of the skin are 10 in. by 10 in., respectively, with an approximate thickness of 0.165 in. The blade stiffener height is 3.5 in. from the flange-to-skin interface to the free end and is 0.440 in. thick. The width of the flanges of the blade stiffener was 2 in., which was determined from the blade centerline to the outermost edge of the flange. During analysis of the ESE model, the deformation and skin-stringer separation was observed to be symmetric about the X-Y and Y-Z planes. Therefore, a quarter model with symmetric boundary conditions was implemented for the DSCE method to decrease the computational time and disk space.

The skin and stiffener flange sections were modeled as composite continuum shell sections with a layup configuration of $[\pm 45^{o}/(0^{o})_{2}/90^{o}/(0^{o})_{2}/\mp 45^{o}]_{3}$ and $[\pm 45^{o}/(0^{o})_{2}/90^{o}/(0^{o})_{2}/\mp 45^{o}]_{4}$, respectively. The stiffener blade was formed by laminates that constitute the two flange sections being brought together along the delta-fillet centerline and has a layup configuration of $[\pm 45^{o}/(0^{o})_{2}/90^{o}/(0^{o})_{2}/\mp 45^{o}]_{8}$. Continuum shell elements, SC8R, were used, and their corresponding lamina properties are shown in Table I. The delta-fillet underneath the blade region was modeled using hexahedron continuum elements with reduced integration, C3D8R, and its corresponding properties are also shown in Table I. In the finite element models presented herein, the bottom supports and top indenters were represented as analytically rigid surfaces. Frictional contact was imposed between the skin and analytically rigid indenters, where a frictional coefficient of 0.33 was assumed. Linear elastic material behavior was assumed in the skin, stiffener, and delta-fillet regions. Translational displacements were constrained at the bottom supports, whereas a downward half-inch displacement was applied with the top indenters to induce skin-stringer separation. Semi-automatic mass scaling was implemented throughout a time period of 0.5 seconds. A stable time increment of 5E-07 seconds was used to minimize the kinetic energy within each model.

Cohesive elements (COH3D8) were applied to model delamination along the entire length of the blade stiffener at the flange-to-skin interface. An element size of 0.01 in. was used. Since the skin, stiffener, delta-fillet were constructed independently, Abaqus tie constraints were used to connect the cohesive elements to the continuum elements. A bilinear traction-separation law was used to represent the interface failure between the skin and stringer. Initiation of damage was determined by using a quadratic maximum stress criterion. Additionally, the B-K fracture criterion was used to simulate the mixed-mode delamination behavior at the skin-to-stringer interface. The cohesive material properties used to model the global delamination behavior is shown in Table II. The flange-to-skin interface fracture properties were obtained from reference [25] and were assumed to be based on an autoclave prepreg material system. These properties are preliminarily used until actual interface properties can be measured.

In this study, four different stitch configurations were investigated and compared between the DSCE and ESE modeling approaches. These configurations are defined as stitched, overstitched (two cases considered), and twice overstitched configurations and are illustrated in Figure 2. The stitch architecture used in this study is a modified chain stitch that allows a one-sided stitch manufacturing process to be used [26]. The stitched seven-point bend configuration represents a single modified chain stitch seam at each flange/skin interface. The overstitched configurations represent multiple modified chain stitching seams that are overlapped. In the ESE method, the stitches were modeled as

truss elements, T2D2, at each stitch location in the through-the-thickness direction. A circular stitch cross-section was assumed with a measured diameter of 0.01 in. In the DSCE, the stitches were represented as COH3D8 elements with a rectangular cross-section of 0.001 in^2. Each stitch element was longitudinally offset by approximately 0.20 in. along the length of the blade. In addition, overstitches were laterally offset by approximately 0.24 in. and 0.47 in. to investigate the effect of additional stitches near the flange ends. The orientation and position of the elements were selected based on estimated measurements within stitched composite preforms. The determination of their stitch element properties is further discussed in detail in the following section.

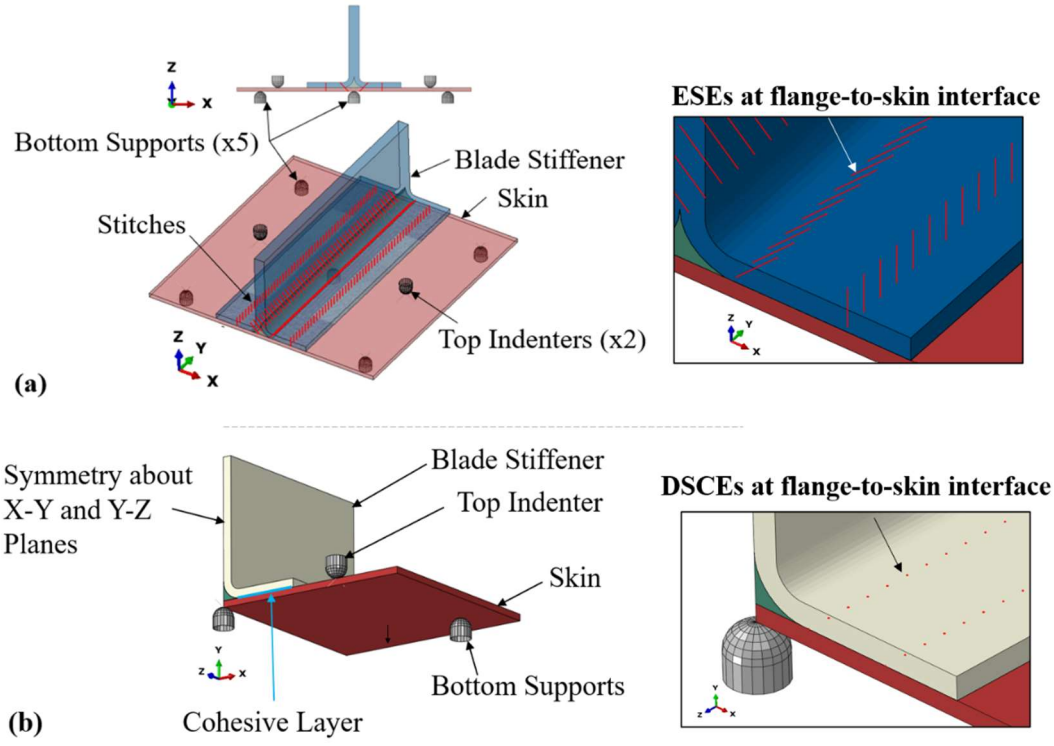

Figure 1. Finite element models using (a) the ESE approach and (b) the DSCE approach.

TABLE I. LAMINA PROPERTIES FOR THE SKIN, STIFFENER, AND DELTA-FILLET.

Region	**E_1 (psi)**	**E_2 (psi)**	**E_3 (psi)**	**$\nu_{12} = \nu_{13} = \nu_{23}$**	**G_{12} (psi)**	**G_{13} (psi)**	**G_{23} (psi)**
Skin	2.13E+07	1.26E+06	-	0.320	7.49E+05	7.49E+05	4.35E+05
Stiffener	2.13E+07	1.26E+06	-	0.320	7.49E+05	7.49E+05	4.32E+05
Delta-Fillet	9.36E+06	9.51E+06	9.51E+06	0.046	7.20E+05	7.20E+05	4.32E+05

TABLE II. FRACTURE PROPERTIES FOR THE FLANGE-TO-SKIN INTERFACE AND DSCE STITCH ELEMENT.

Region	K_I (lbf/in^3)	K_{II} (lbf/in^3)	G_{IC} (lbf/in)	G_{IIC} (lbf/in)	σ_C (lbf/in^2)	τ_C (lbf/in^2)	η_{BK}
Flange-to-Skin Interface	1.80E+08	1.3E+08	1.370	4.22	9.04E+03	1.35E+04	2.07
DSCE (G_A)	2.25E+08	1.50E+08	1450	850	2.10E+05	1.15E+05	2.00
DSCE (G_B)	4.35E+07	2.65E+07	4100	3100	5.75E+05	3.75E+05	2.00

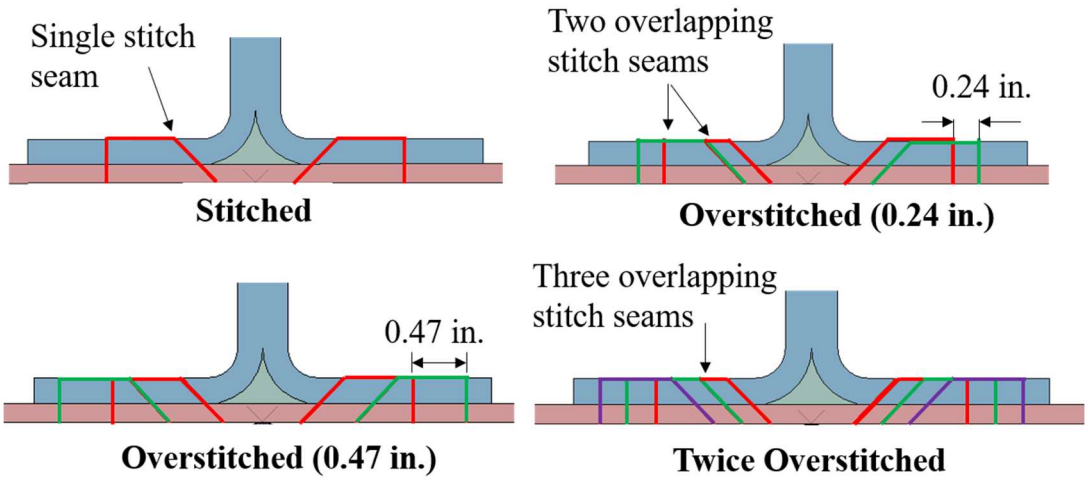

Figure 2. Stitch configurations using the one-sided stitching process.

DETERMINATION OF STITCH ELEMENT BEHAVIOR

In this study, the constitutive bridging behavior of the through-the-thickness reinforcements within the seven-point bend finite element models were determined based on interlaminar tensile and shear tests that contained multiple stitches [6]. The reference [5] study uses a Kevlar thread that is similar in strength to a 1200 Denier Vectran™ thread [27] and is used in the present study. The experimental data included only considers stitches that are orthogonal to the delaminated plane. Differing load-displacement responses may be obtained from angled stitches [13]. Therefore, additional interlaminar tensile and shear tests need to be conducted to account for the effect of the angle of the stitch. The load-displacement response from these experiments is shown in Figures 3(a), 3(b), and 4. Initially, a relatively linear response is observed as the applied displacement increases. A decrease in the slope is observed at an inflection load (P_A), which is followed by a linear increase in the load until an abrupt stitch failure occurs at the maximum load (P_B).

The selection of the bridging law plays a significant role in predicting failure when large-scale bridging conditions occur. Studies [28,29] have shown that superposing two bilinear traction-separation laws can accurately predict crack growth behavior with large-scale fiber filament bridging. Using the DSCE approach, two bilinear traction-separation laws (G_A and G_B) were superposed to be representative of the experimental load-displacement response of stitches subjected to tensile and shear

loading, as shown in Figures 3(a) and 3(b). The fracture energies, penalty stiffnesses, and maximum elastic stresses of both traction separation laws were manually calibrated to the experimental data. The superposed traction-separation law fracture properties that use the DSCE method are shown in Table II.

The total bridging energy represents the cumulative energy of the stitch during interlaminar testing [26] and is characterized by the area under the load-displacement curve. The total bridging energy E_T can be represented by the summation of initial (E_A) and secondary (E_B) bridging energies. The initial and secondary energies are each represented as a bilinear load-displacement response corresponding to each traction-separation law. Each bilinear response is initially linear until a maximum load is achieved. Afterward, a linear decrease in the load-displacement response is observed until a zero load is attained. The summation of each bilinear response develops a trilinear load-displacement behavior that is representative of stitches subjected to tensile and shear loads. The bilinear response of the initial bridging energy (E_A) was used to establish the initial linear slope and inflection load (P_A) of the total bridging response (E_T). However, the inflection load (P_A) is influenced by both bilinear laws since each law begins from a zero displacement. Furthermore, the bilinear response of the secondary energy (E_B) is primarily used to establish the change in stiffness (load/displacement) and the maximum load (P_B) when interfacial debonding and stitch fiber fracture occur.

The predicted load-displacement response as a function of the applied displacement for an ESE element subjected to tensile loads is shown in Figure 4. The ESE method generally shows good agreement with interlaminar tensile test experimental data. However, it is observed that the predicted response using an ESE element slightly underpredicts the experimental data by approximately 4%.

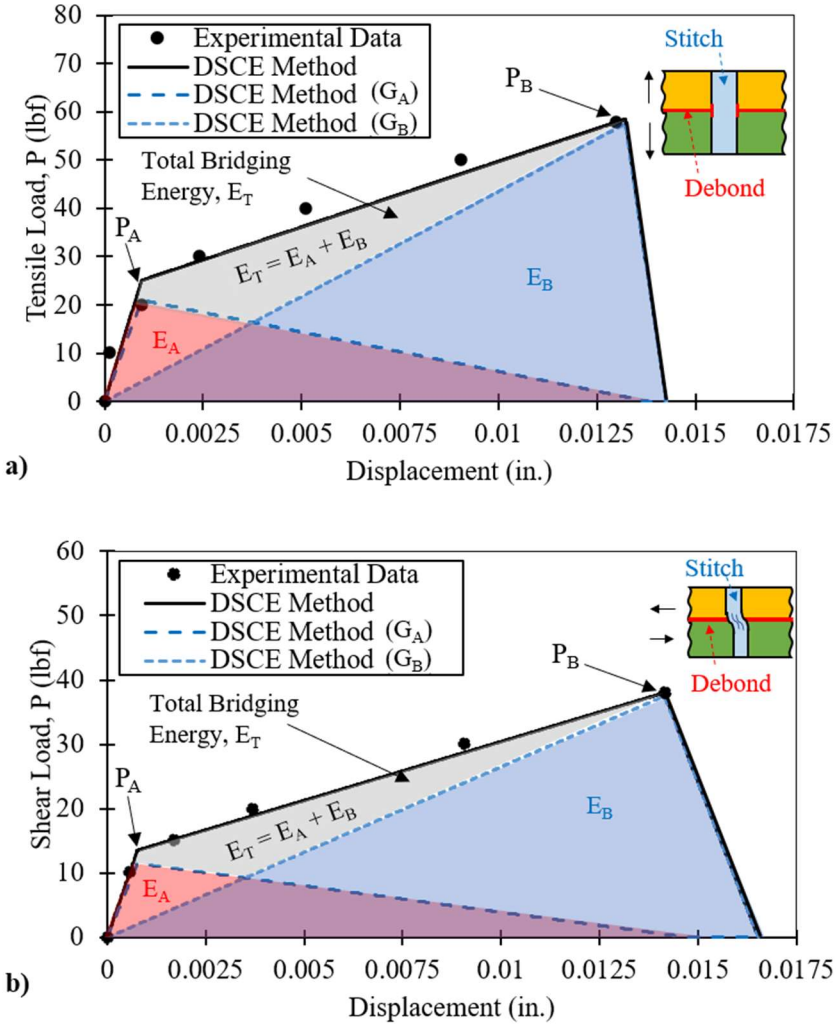

Figure 3. Single stitch load-displacement (a) tensile and (b) shear responses using the DSCE method. Experimental data was taken from [6] and [12], respectively.

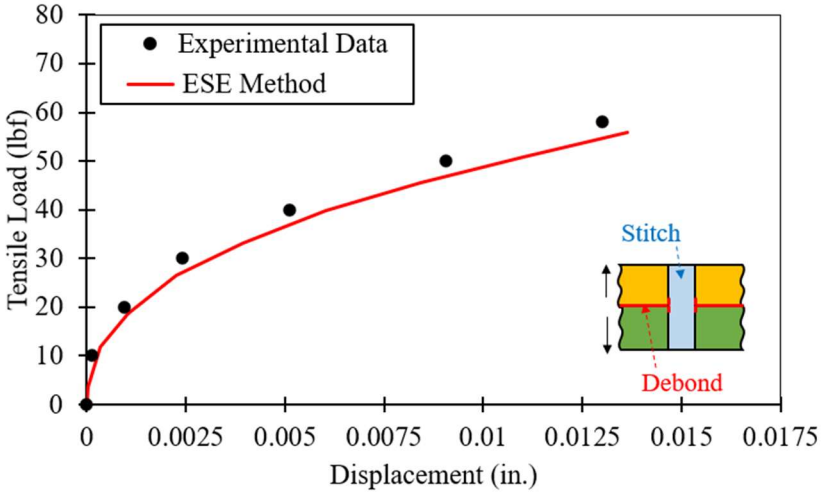

Figure 4. Single stitch load-displacement tensile response using the ESE method. Experimental data and schematic were taken from [6] and [12], respectively.

RESULTS AND DISCUSSION

The through-the-thickness reinforcements significantly impact the load magnitude and slope (stiffness) of the predicted load-displacement response of the blade stiffened panels subjected to seven-point bending. The load as a function of the applied displacement for the selected stitch configurations and modeling strategies is shown in Figure 5. Filtering was not conducted on the load-displacement response. Solid and dotted lines represent the DSCE and ESE modeling approaches, respectively, for each stitch configuration. The solid black line representing the unstitched FEM does not contain stitch elements. Initially, the applied displacement increases the reacted load linearly with no observed difference before crack initiation between each seven-point bend specimen of different stitch configurations. At crack initiation, the stiffness decreases with an increase in the applied displacement. After crack initiation, the overstitched (0.47 in.) and twice overstitched stiffened panels equally develop a maximum load of approximately 41% and 18% greater than the unstitched and single stitch counterparts, respectively. In addition, the ESE method shows reasonable agreement to the DSCE method with a maximum deviation of 5% difference at the maximum applied load.

The stitches were not predicted to influence the load-displacement response until the bridging of through-the-thickness reinforcement occurs, which results in an increase in the stiffness shortly after delamination initiation. These critical displacements are denoted as the circular points depicted in Figure 5. The overstitched and twice overstitched stiffened panels require less applied displacement than the stitched stiffened panels to incur a stiffness increase. This behavior is attributed to stitches being closer to the flange edge, where delamination at the skin-stringer interface begins to initiate. Intuitively, through-the-thickness reinforcements close to the outermost edge of the flange can maximize the resistance to delamination. However, through-the-thickness reinforcements directly near the edge can lead to stress concentrations associated with the resin-rich pockets within the vicinity of the stitches [31], which was not considered herein. Therefore, a determination of the optimal distance to the flange edge needs to be further investigated.

A reduction in stiffness was observed after delamination initiation. The relative stiffnesses, K_1 and K_2, represent the stiffness of the load-displacement response before and after delamination, respectively. These relative stiffnesses for each stitch configuration and modeling approach are shown in Figure 6. Before delamination, the K_1 stiffness using each method does not show a significant change between each stitch configuration. After delamination occurs, a 92% retainment in stiffness is predicted for highly stitched specimens (overstitched and twice overstitched). This retainment in stiffness may imply that the through-the-thickness reinforcements act as a fail-safe mechanism to allow the skin to retain greater loads during delamination after a post-buckling event. The ESE method develops approximately 3% to 8% greater stiffness than the DSCE method for each configuration, which may be associated with differences in boundary conditions between the two methods. Symmetric boundary conditions was only employed for the DSCE approach.

The crack length was calculated for select applied displacements and measured from the flange end to the crack front. The predicted crack length as a function of the applied displacement for select stitch configurations and modeling strategies is shown in

Figure 7. Stitches were not observed to fail during each simulation. For the unstitched specimen, an initial linear increase in the crack length was observed until the crack front approached the delta-fillet region. Afterward, a reduction in the crack length was observed and converged to a crack length of 1.50 in. For the stitched specimens, a linear increase in the crack length was observed until the through-the-thickness reinforcements began to bridge the delaminated interface. The unstitched specimen was predicted to have 35% greater crack length than the overstitched and twice overstitched specimens. However, a reduction of 48% in crack length is achieved when the through-the-thickness reinforcements are closer to the flange ends (overstitched – 0.47 in. and twice overstitched). The ESE method overestimates the crack length by approximately 13% as compared to the DSCE approach. The differences between both methodologies can be attributed to the additional shear loading capability that is predicted using the DSCE approach. This shear loading capability represents the lateral stitch deflection through the surrounding matrix and flexural splitting of the stitches near the skin-stringer delaminated interface [14,32]. However, it is important to note that the ESE approach uses only one element in the through-the-thickness direction. Thus, reducing the element length near the delaminated interface may be necessary to represent interfacial shear of through-the-thickness reinforcements accurately. Further investigation is needed to determine the proper element length near delaminated interfaces that are subjected to high interfacial shear conditions.

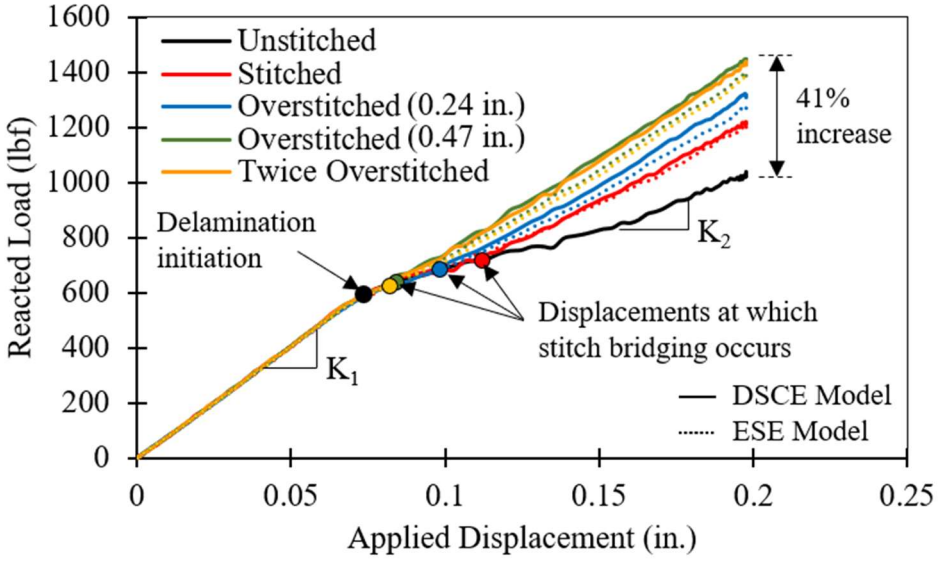

Figure 5. The predicted load as a function of the applied displacement for unstitched, stitched, and overstitched seven-point bend specimens.

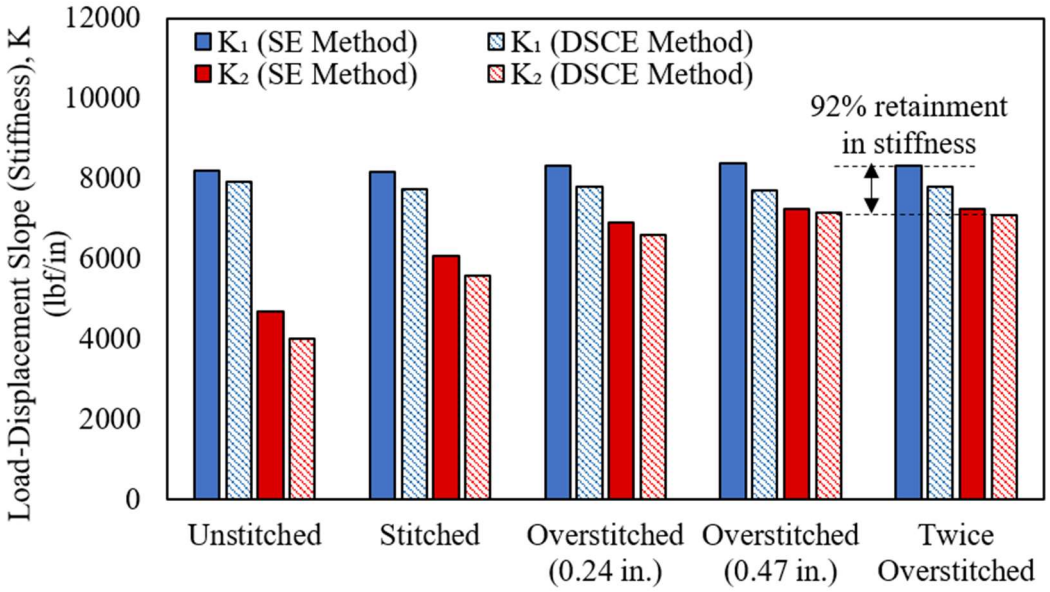

Figure 6. Calculated stiffness for select stitch configurations and modeling strategies.

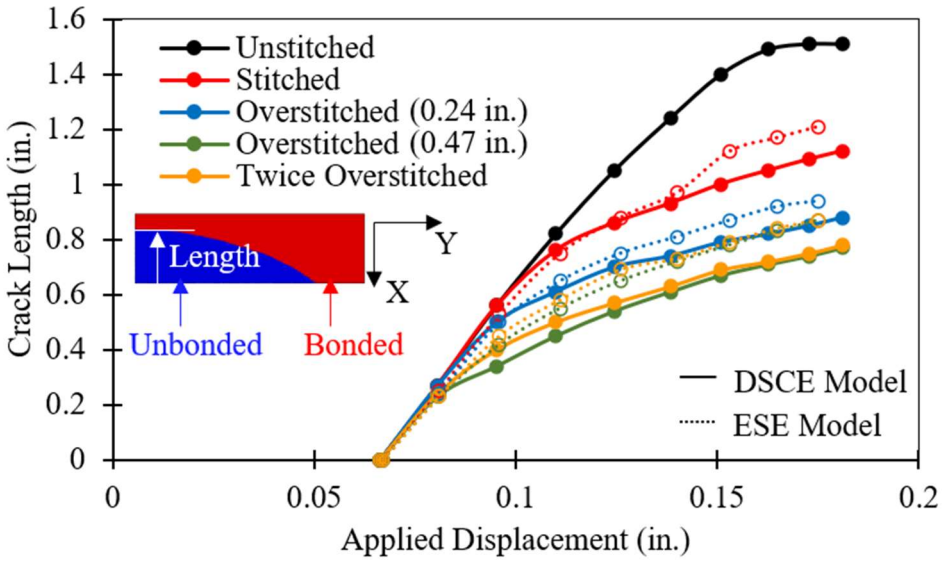

Figure 7. The predicted crack length as a function of the applied displacement for unstitched, stitched, and overstitched seven-point bend specimens.

CONCLUSIONS

In this study, the delamination behavior in unstitched and stitched stiffened panels subjected to seven-point bend loads was investigated. A discrete superposed cohesive element, or DSCE, approach was applied to capture the physical damage mechanisms of stitches subjected to mixed-mode stresses, which is not entirely represented by using the traditional one-dimensional ESE approach. The DSCE approach uses superposed traction-separation laws to present the trilinear load-displacement behavior of stitches subjected to tensile and shear loads. The traction-separation laws were independently

calibrated using interlaminar tension and shear tests, and the mixed-mode behavior was represented using a B-K fracture criterion. Load-displacement and crack growth results using DSCE approach were compared to a model using the ESE approach. The predicted load-displacement response between the spring element method and the DSCE method showed good agreement; however, the ESE method overestimated the crack growth as compared to the DSCE approach. It was observed that having stitches near the flange ends resists the greatest amount of skin-stringer separation using a single overstitched approach. Stitches were not observed to fail during skin-stringer separation. No significant difference was observed in crack growth for stiffeners that were overstitched or twice overstitched. The DSCE method presented in this study provides a pathway to model the mixed-mode behavior of through-the-thickness reinforcements subjected to mixed-mode stresses in stitched, blade stiffened composite panels.

ACKNOWLEDGEMENTS

The authors would like to gratefully acknowledge Dr. Andrew Bergan and Dr. Carlos Dávila for their valuable input and review of this manuscript.

REFERENCES

[1] Mouritz, A. P., Leong, K. H., and Herszberg, I. "A Review of the Effect of Stitching on the In-Plane Mechanical Properties of Fibre-Reinforced Polymer Composites." *Composites Part A: Applied Science and Manufacturing*, Vol. 28, No. 12, 1997, pp. 979–991. https://doi.org/10.1016/S1359-835X(97)00057-2.

[2] Drake, D. A., Sullivan, R. W., Lovejoy, A. E., Clay, S. B., and Jegley, D. C. "Influence of Stitching on the Out-of-Plane Behavior of Composite Materials – A Mechanistic Review." *Journal of Composite Materials*, Vol. 55, No. 23, 2021, pp. 3307–3321. https://doi.org/10.1177/00219983211009290.

[3] Velicki, A., and Jegley, D. C. PRSEUS Structural Concept Development. In *52nd Aerospace Sciences Meeting*, American Institute of Aeronautics and Astronautics, 2014.

[4] Jegley, D., Rouse, M., Przekop, A., and Lovejoy, A. *The Behavior of a Stitched Composite Large-Scale Multi-Bay Pressure Box*. Publication NASA/TM-2016-218972. NASA Langley Research Center, Hampton, VA, 2016, pp. 1–93.

[5] Abaqus 2021. *Abaqus User Manual*. Dassault Systèmes.

[6] Glaessgen, E., Raju, I., and Poe, Jr., C. Fracture Mechanics Analysis of Stitched Stiffener-Skin Debonding. In *39th AIAA/ASME/ASCE/AHS/ASC Structures, Structural Dynamics, and Materials Conference and Exhibit*, American Institute of Aeronautics and Astronautics, 1998.

[7] Seon, G., Makeev, A. V., Shonkwiler, B., Schaefer, J., and Justusson, B. An Integrated Approach for Characterizing Non-Crimp Fabric Composites with Interlaminar Stitching Reinforcement. In *AIAA Scitech 2021 Forum*, American Institute of Aeronautics and Astronautics, 2021.

[8] Tan, K. T., Watanabe, N., Sano, M., Iwahori, Y., and Hoshi, H. "Interlaminar Fracture Toughness of Vectran-Stitched Composites - Experimental and Computational Analysis." *Journal of Composite Materials*, Vol. 44, No. 26, 2010, pp. 3203–3229. https://doi.org/10.1177/0021998310369581.

[9] Sun, S., Wang, X., Liang, J., Yang, R., and Zhao, Y. "Analysis on Fracture Behaviour of Stitched Foam Sandwich Composites Using Interlaminar Tension Test." *Journal of Sandwich Structures & Materials*, Vol. 24, No. 3, 2022, pp. 1515–1534. https://doi.org/10.1177/10996362211063154.

[10] Tabatabaei, S. A., Lomov, S. V., and Verpoest, I. "Assessment of Embedded Element Technique in Meso-FE Modelling of Fibre Reinforced Composites." *Composite Structures*, Vol. 107, 2014, pp. 436–446. https://doi.org/10.1016/j.compstruct.2013.08.020.

[11] Iwahori, Y., Nakane, K., and Watanabe, N. “DCB Test Simulation of Stitched CFRP Laminates Using Interlaminar Tension Test Results.” *The Sixteenth International Conference on Composite Materials with Regular Papers*, Vol. 69, No. 14, 2009, pp. 2315–2322. https://doi.org/10.1016/j.compscitech.2008.12.018.

[12] Bergan, A. *Test and Analysis of Stitched Composite Structures to Assess Damage Containment Capability*. Dissertation. Drexel University, 2014.

[13] Justusson, B., and Schaefer, J. D. Development of Analytical Capabilities for Through Thickness Composite Structure Design and Substantiation. In *AIAA SCITECH 2022 Forum*, American Institute of Aeronautics and Astronautics, 2021.

[14] Cartié, D. D. R., Cox, B. N., and Fleck, N. A. “Mechanisms of Crack Bridging by Composite and Metallic Rods.” *Composites Part A: Applied Science and Manufacturing*, Vol. 35, No. 11, 2004, pp. 1325–1336. https://doi.org/10.1016/j.compositesa.2004.03.006.

[15] Drake, D. A., Sullivan, R. W., and Clay, S. “On the Use of a Trilinear Traction-Separation Law to Represent Stitch Failure in Stitched Sandwich Composites.” *Journal of Sandwich Structures & Materials*, Vol. 24, No. 2, 2022, pp. 1367–1384. https://doi.org/10.1177/10996362211042929.

[16] Ranatunga, V., and Clay, S. B. “Cohesive Modeling of Damage Growth in Z-Pinned Laminates under Mode-I Loading.” *Journal of Composite Materials*, Vol. 47, No. 26, 2013, pp. 3269–3283. https://doi.org/10.1177/0021998312464078.

[17] Herwan, J., Kondo, A., Morooka, S., and Watanabe, N. “Finite Element Analysis of Mode II Delamination Suppression in Stitched Composites Using Cohesive Zone Model.” *Plastics, Rubber and Composites*, Vol. 44, No. 9, 2015, pp. 390–396. https://doi.org/10.1179/1743289815Y.0000000035.

[18] Bianchi, F., and Zhang, X. “A Cohesive Zone Model for Predicting Delamination Suppression in Z-Pinned Laminates.” *Composites Science and Technology*, Vol. 71, No. 16, 2011, pp. 1898–1907. https://doi.org/10.1016/j.compscitech.2011.09.004.

[19] Wood, M. D. K., Sun, X., Tong, L., Luo, Q., Katzos, A., and Rispler, A. “A New ENF Test Specimen for the Mode II Delamination Toughness Testing of Stitched Woven CFRP Laminates.” *Journal of Composite Materials*, Vol. 41, No. 14, 2007, pp. 1743–1772. https://doi.org/10.1177/0021998306069890.

[20] Leone, F., Song, K., Johnston, W., Rose, C., Jackson, W., Kosztowny, C., and Davila, C. Test/Analysis Correlation of Damage States in Post-Buckled Stiffened Validation Building Block Specimens. Presented at the 34th ASC Conference, Atlanta, GA, 2019.

[21] Wanthal, S., Schaefer, J., Justusson, B., Hyder, I., Engelstad, S., and Rose, C. Verification and Validation Process for Progressive Damage and Failure Analysis Methods in the NASA Advanced Composites Consortium. Presented at the The 32nd American Society for Composites Technical Conference, West Lafayette, IN, 2017.

[22] van Rijn, J. C. F. N., and Wiggenraad, J. F. M. *A Seven-Point Bending Test to Determine the Strength of the Skin-Stiffener Interface in Composite Aircraft Panels*. Publication NLR-TP-2000-044. National Aerospace Laboratory NLR, 2000.

[23] Leone, F. A., Jegley, D. C., and Linton, K. A. Compressive Loading and Modeling of Stitched Composite Stiffeners. In *57th AIAA/ASCE/AHS/ASC Structures, Structural Dynamics, and Materials Conference*, American Institute of Aeronautics and Astronautics, 2016.

[24] Yovanof, N., and Jegley, D. Compressive Behavior of Frame-Stiffened Composite Panels. In *52nd AIAA/ASME/ASCE/AHS/ASC Structures, Structural Dynamics and Materials Conference*, American Institute of Aeronautics and Astronautics, 2011.

[25] Kosztowny, C., Davila, C. G., Song, K., Rose, C. A., and Jackson, W. Experimental and Numerical Analysis of Skin-Stiffener Separation Using a Seven-Point Bend Configuration. Presented at the AIAA Scitech Forum, San Siego, CA, 2019.

[26] Trabelsi, W., Michel, L., and Othomene, R. “Effects of Stitching on Delamination of Satin Weave Carbon-Epoxy Laminates Under Mode I, Mode II and Mixed-Mode I/II Loadings.” *Applied Composite Materials*, Vol. 17, No. 6, 2010, pp. 575–595. https://doi.org/10.1007/s10443-010-9128-0.

[27] Tan, K., Watanabe, N., and Iwahori, Y. “Stitch Fiber Comparison for Improvement of Interlaminar Fracture Toughness in Stitched Composites.” *Journal of Reinforced Plastics and Composites*, Vol. 30, No. 2, 2011, pp. 99–109. https://doi.org/10.1177/0731684410383065.

[28] Dávila, C. G., Rose, C. A., and Camanho, P. P. “A Procedure for Superposing Linear Cohesive Laws to Represent Multiple Damage Mechanisms in the Fracture of Composites.” *International*

Journal of Fracture, Vol. 158, No. 2, 2009, pp. 211–223. https://doi.org/10.1007/s10704-009-9366-z.

[29] Bergan, A., Dávila, C., Leone, F., Awerbuch, J., and Tan, T.-M. "A Mode I Cohesive Law Characterization Procedure for Through-the-Thickness Crack Propagation in Composite Laminates." *Composites Part B: Engineering*, Vol. 94, 2016, pp. 338–349. https://doi.org/10.1016/j.compositesb.2016.03.071.

[30] Tan, K. T., Watanabe, N., and Iwahori, Y. "Experimental Investigation of Bridging Law for Single Stitch Fibre Using Interlaminar Tension Test." *Composite Structures*, Vol. 92, No. 6, 2010, pp. 1399–1409. https://doi.org/10.1016/j.compstruct.2009.11.018.

[31] Liotier, P.-J., Vautrin, A., and Beraud, J.-M. "Microcracking of Composites Reinforced by Stitched Multiaxials Subjected to Cyclical Hygrothermal Loadings." *Composites Part A: Applied Science and Manufacturing*, Vol. 42, No. 4, 2011, pp. 425–437. https://doi.org/10.1016/j.compositesa.2011.01.003.

[32] Cox, B. N. "Snubbing Effects in the Pullout of a Fibrous Rod from a Laminate." *Mechanics of Advanced Materials and Structures*, Vol. 12, No. 2, 2005, pp. 85–98. https://doi.org/10.1080/15376490490493899.